M 2017

U.PORTO
FEUP FACULDADE DE ENGENHARIA
UNIVERSIDADE DO PORTO

USE OF ADDITIVE MANUFACTURING IN CHEMICAL ENGINEERING

NÚRIA FILIPA BASTOS REBELO

DISSERTAÇÃO DE MESTRADO APRESENTADA
À FACULDADE DE ENGENHARIA DA UNIVERSIDADE DO PORTO EM
ENGENHARIA QUÍMICA

Master in Chemical Engineering

Use of additive manufacturing in chemical engineering

A Master's dissertation

of

Núria Filipa Bastos Rebelo

Developed within the course of dissertation

held in

SINTEF

Supervisor at FEUP: **Prof. Manuel Alves**

Supervisor at SINTEF: **Dr. Carlos Grande**

Departamento de Engenharia Química

July of 2017

Acknowledgements

First, I want to thank FEUP and SINTEF for the opportunity presented.

I want to thank Dr. Carlos Grande for all the support, advices and help during all the internship. Also, to everyone in the company for the warm welcoming and availability to help, with a special thanks to Kari Anne Andreassen.

I thank Prof. Manuel Alves for all the help and patience.

I also want to thank my family for all the support and incentive.

I also thank my friends for always being available for support, advices and jokes.

This work was developed within the PRINTCR3DIT project. This project has received funding from the European Union's Horizon 2020 research and innovation programme under grant agreement No. 680414.

Abstract

Packed bed reactors have an important role in the chemical industries as they provide a high contact area between the fluid and the solid. With the advances in the 3D printing technology new structured packings can be designed, produced and tested, all while maintaining a relatively low price and a fast production process. Most importantly, the main advantage of this approach is to produce tailored packings for specific problems in a given reaction.

In this work, the pressure drop and heat transfer properties of seven iso-reticular cubic cell metallic foams were tested. To measure the pressure drop, experiments with each foam were made in air flow varying the gas superficial velocity from 0 to 20 $m \cdot s^{-1}$. In addition, global heat transfer coefficients to an air stream were measured when the reactor is heated in a water bath.

In both set of experiments, the porosity, cell width, strut thickness and the angular rotation of the cubic matrices were the parameters studied. The pressure drop and the global heat transfer coefficient decrease with the increase of porosity, the increase of cell width, and the decrease of strut thickness, while are not affected significantly by the angle of the matrix.

Keywords (theme): packed bed, 3D printed, pressure drop, heat transfer

Resumo

Os reatores de leito fixo têm uma grande importância na indústria Química, uma vez que possibilitam uma elevada área de contacto entre o fluído e o sólido. Com os avanços na impressão 3D, novos tipos de empacotamento estruturado podem ser criados, produzidos e testados, mantendo um preço relativamente baixo e uma produção rápida. Mais importante, a maior vantagem desta abordagem é a produção de um empacotamento específico para uma dada reação.

Neste trabalho mediu-se a queda de pressão e o coeficiente global de transferência de calor em sete leitos de células cúbicas metálicas. Para a medição da queda de pressão, cada reator foi testado com escoamento de ar, variando a velocidade superficial entre 0 e 20 $m \cdot s^{-1}$. Adicionalmente, mediu-se o coeficiente global de transferência de calor para o escoamento de ar quando o reator é aquecido num banho de água.

Em ambos os casos foi estudado o efeito a porosidade, tamanho da célula, espessura dos ligamentos e o ângulo de rotação das células cúbicas que constituem o leito poroso. Os resultados obtidos mostram que a queda de pressão e o coeficiente global de transferência de calor apresentam comportamentos semelhantes quando variados os parâmetros mencionados, observando-se que ambos diminuem com o aumento da porosidade, com o aumento do tamanho da célula e com a diminuição da espessura dos ligamentos, sendo pouco sensíveis à variação dos ângulos das células cúbicas.

Palavras chave (tema): reator de leito fixo, impressão 3D, queda de pressão, transferência de calor

Declaration

I hereby declare, on my word of honour, that this work is original and that all non-original contributions were properly referenced with source identification.

Index

List of figures

List of tables

Notation and Glossary

A	Area	m^2
ΔT	Change in the fluid temperature	K
e	Cell strut thickness	m
d	Diameter	m
K_1	Ergun's constant for laminar flow	
K_2	Ergun's constant for turbulent flow	
U	Global heat transfer coefficient	$W \cdot m^{-2} \cdot K^{-1}$
$\dot{Q}$	Heat transfer rate	W
L	Length of the reactor	m
ΔT_{LN}	Log-mean temperature difference	K
$\dot{m}$	Mass flow rate	$kg \cdot s^{-1}$
ΔP	Pressure drop	Pa
C_p	Specific heat	$J \cdot kg^{-1} \cdot K^{-1}$
v	Superficial velocity	$m \cdot s^{-1}$
T	Temperature	K

Greek Letters

ρ	Density	$kg \cdot m^{-3}$
e	Porosity	
μ	Viscosity	Pa·s

Indexes

in	Entrance of packed bed
out	Exit of packed bed
f	Fluid
int	Internal cell unit
r	Reactor
p	Spherical particle
wall	Wall of the packed bed

List of Acronyms

ABS	Acrylonitrile Butadiene Styrene
AM	Additive Manufacturing
P2VP	Poly(2-vinylpyridine)
STL	stereolithography file format
SLA	Stereolithography technique
3D	Three dimensional

1 Introduction

1.1 Framing and presentation of the work

Three dimensional (3D) printing, also known as additive manufacturing (AM), allows to redesign, and create new products in a short time. Without the same constrains of intensive manual labor, 3D printing allows to create a custom-build piece with specific characteristics in a cheap and fast way (Cotteleer and Joyce 2014).

3D printing has been largely used in several industries for production of models and prototypes during the product development phase, parts for pilot series production in medical, automotive, and aerospace industry, short series production where tooling cost for casting and injection molding would be too high, and parts of high geometrical complexity which cannot be produced by means of conventional manufacturing (Metal AM s.d.).

In the chemical engineering field, some applications of this technology are 3D printed polypropylene reactors that perform close to the classical stainless-steel reactors at 150 ºC, or the screen-printable electronic inks that can be used in smart clothing and be equipped with sensors from temperature to electrocardiogram (Van Thienen, et al. 2016). Besides these applications, 3D printing technology can also change dramatically the industry since it has the potential to produce a reactor for a specific reaction kinetics or residence time of the reaction (Cotteleer and Joyce 2014).

In this work, tailored-made packed beds were printed using direct laser metal sintering and will be studied as an alternative for typical packed beds.

Packed bed reactors have a major impact in the chemical industry, leading the reaction engineering and with a wide variety of other applications, such as in absorption, ion-exchange resin beds and heat exchangers. The properties of this type of reactor depend entirely on the packing chosen and how it was loaded, as the porosity of the bed will define the pressure drop and the superficial area of the particles will influence the heat transfer.

Pellets are usually used as the packing material, yet they present the problem of a low bed porosity, which causes a higher pressure drop, and since the particles only have contact points the effective thermal conductivity of the system decreases.

To overcome these problems new packings were studied, such as open cell foams. The high surface area to volume ratio, as well as enhanced flow mixing,

attractive stiffness and strength along with the open porosity and low relative density makes the metal foam thermal management devices efficient, compact and light-weight and with low pressure drop.

This thesis will focus on the characterization of packed beds using iso-reticular open cell foams created by 3D printing, namely in the study of the pressure drop and the heat transfer coefficient between different foams.

1.2 Presentation of the company

SINTEF was founded in 1950. With 2000 employees, SINTEF is the fourth largest independent contract research organization in Scandinavia and the fourth in Europe. It is a multidisciplinary research organization with international top-level expertise in the fields of technology, natural sciences, medicine and social sciences. The strategic focus areas are: renewable energy, environmental technology; oil and gas; ocean space technology; health and welfare and enabling technologies.

SINTEF develops society through research and innovation. It creates value and develops solutions to challenges faced by society and actively communicate its knowledge, solutions, and recommendations.

SINTEF vision is “Technology for a better society”.

The work was carried out the Division of Materials and Chemistry in Oslo as a collaboration between the Sorbent Technologies and Process Intensification and Catalysis R&D groups. The work was conducted within the PRINTCR3DIT EU project coordinated by SINTEF and where FEUP is one of the partners.

1.3 Contributions of the Work

The main work developed was the characterization of 3D printed packed beds. The main topics studied included the pressure drop and heat transfer coefficient. To accomplish this study, new experimental installations were designed, installed and tested. The experiments were then made by modifying several parameters in the foams. The data was treated and is presented in this work, such as the influence of each parameter in the overall results. This analysis of the data allows to characterize the printed packed beds.

1.4 Organization of the thesis

The thesis will focus on the study of an alternative for packed beds made by using additive manufacturing. Firstly, there will be a study of the pressure drop in packed bed reactors, and subsequently there will be a study of heat transfer inside this type of reactor.

The next chapter, Context and State of Art, will present an introduction to the Additive Manufacturing and its evolution so far, followed by the description of different types of packed beds existing in the industry. Both of these topics are relevant to the context of this thesis.

Next, in the methods and materials chapter, the procedures used in the experiments and the material used will be described.

The results and discussion will present the data acquired in the experiments followed by a discussion about its validity and expectations.

Finally, the conclusions are presented followed by a critical assessment of the work developed and possible improvements.

2 Context and State of the art

2.1 Additive Manufacturing

Additive manufacturing (AM) is the process of creating physical products through the addition of materials, usually layer by layer, also known as 3D printing. This technology allows to create a custom-built piece with specific characteristics in a cheap and fast way (Cotteleer and Joyce 2014).

The technique of 3D printing has been evolving for over three decades with the use of new and improved materials, the improvement of the technique itself and the development of new ones. Some examples of systems used are fused deposition, selective heat or laser sintering, photopolymerization and thin-film lamination.

The first 3D printing process was announced in April of 1981 in a Japanese edition of the IEICE Transactions on Electronics, volume J64-C, and it was entitled “A scheme for three-dimensional display by automatic fabrication of three-dimensional model”. This technique consisted in using controlled ultraviolet light exposure on a photo-hardening polymer.

The next big step for 3D printing was the creation of the stereolithography technique (SLA). In 1984, the inventors Alain Le Méhauté, Olivier de Witte, and Jean Claude André filed a patent for the SLA and three weeks later Chuck Hull filed his own patent for the SLA. The French inventors abandoned the patent application (by the French General Electric Company and CILAS) because of “lack of business perspective”. The patent of the SLA was awarded to Hull, even though his most significant contribution was the stereolithography file format (STL), file developed by him and that is still used widely by 3D printing software.

The use of metals as printing materials started in mid-1990s even though most productions still relied on more traditional cutting, casting or stamping processes. Usually the creation of 3D metal objects is associated with removing material from a larger block using an automated cutting tool. So, when sintering was developed, more akin to welding, a more complex number of geometries and parts became available to manufacture. Also, the implementation of sacrificial and support materials, by the early 2000s, enabled the production of additional geometries.

While the costs of using AM have been a setback and a limitation in its use, in 2005 emerged the first low cost 3D printer, RepRap, capable of replicating itself. The

technology was developed by Dr. Adrian Bowyer after the patents in additive technology started to expire. Naturally, low-cost 3D printing companies started to emerge.

In the past three years the AM market has grown with an average annual growth rate of 33.8 %. Increasing from just over 750 million dollars in 2005 to over 5.1 billion in 2016 (Sivertsen 2016).

Nowadays, the use of this manufacture technique can be environmental friendly since it helps reducing the amount of waste during manufacturing, because is an additive process, creates lightweight components that reduce material consumption in transportation and in the supply chain and the capacity to optimize geometries, and inventory waste reduction due to the ability to create spare parts on-demand. For example, the aerospace industry is an excellent example where the AM technology is ideal, since it requires the production of a small number of highly complex aircraft components (Ford and Despeisse 2016). The GE aviation is currently producing the fuel nozzle injector for the LEAP engine through AM, and this specific piece can be seen in *Figure 1*. Each piece is 25 % lighter and five times more durable when compared to conventional casting processes, which required welding and brazing 20 different parts to obtain the same piece. Furthermore, this company is already investing in a new engine in which 35 % of the components will be produced using AM. This project started in 2015 and is expected to be tested by the end of 2017 (GE Additive 2016). Besides GE, other industries have already adopted this technique for mass production such as Ford, Mattel, and Airbus (Dodziuk 2014). Furthermore, the range of applications using this technology is still increasing and has great potential.

Figure 1 - Nozzle injector produced by additive manufacture (Rockstroh, et al. 2013)

In fact, the use of AM in industries will have a big role in the fourth industrial revolution, a campaign being developed by the German government. The fourth industrial revolution also known as Industry 4.0 intends to put together several digital and physical advanced technologies to form a better physical-to-digital-to-physical connection. It has the potential to transform the industry by promoting strategic growth and streamlining operations by using relevant advanced technologies such as the Internet of Things, advanced materials, additive manufacturing, advanced analytics, artificial intelligence, and robotics. The combination of these have reached a level of cost and performance that enables extensive applications, one example being a company that is fully automated to produce personalized liquid soap. The client places an order for a customized soap which are turned into tags with radio-frequency. These tags are attached to the soap containers and when read informs the equipment on the production line, via wireless network connections, about the aspired composition of the soap and packaging and so allowing customization without human involvement (Van Thienen, et al. 2016).

Even though a lot of innovation is happening in the AM, the expiration of patents has been and still is a major driver in the industry. Allowing this technique to be available to small businesses have resulted in new markets, techniques, tools and new applications emerged (Sivertsen 2016).

More than just changing the infrastructures and methods of production, 3D printing can also change the materials used. Recently, there has been an increase of interest in stimuli-responsive materials, that change their structure when in contact with an external stimulus. Also known as smart material, it can be stimulated by pH, temperature, or light. These have developed the term 4D printing, that consists precisely in structures that can transform in a preprogrammed way in response to a stimulus. For example: artificial bones printed using polycaprolactone/hydroxyapatite, which successfully mimicked the biomechanics of natural bones or the use of poly(2-vinylpyridine) (P2VP) reinforced with Acrylonitrile Butadiene Styrene (ABS) for production of pH response polymer or even just the use of 3D printed P2VP as a mediator in heterogeneous catalysis, which, while achieving the same reaction efficiency, eliminates the need to use harmful chemicals, and streamlines operational time and costs needed for catalyst separation and recycling. Even though the 3D printing materials are evolving, there are still a limited number of functional polymers that can be used. Expanding this list will enable even more applications to emerge (Nadgorny, et al. 2016).

In this work, different packed beds were printed through laser metal sintering. Firstly, the object is divided into several layers that will be built one after the other. Sintering happens when a laser touches a thin layer of the metal alloy and brings its temperature above the melting point. A new thin layer of the metal is spread continuously above the previous sintered layer and the laser will systematically touch the correct spots of each layer and sinter the object together. A schematic of the process is shown in *Figure 2*.

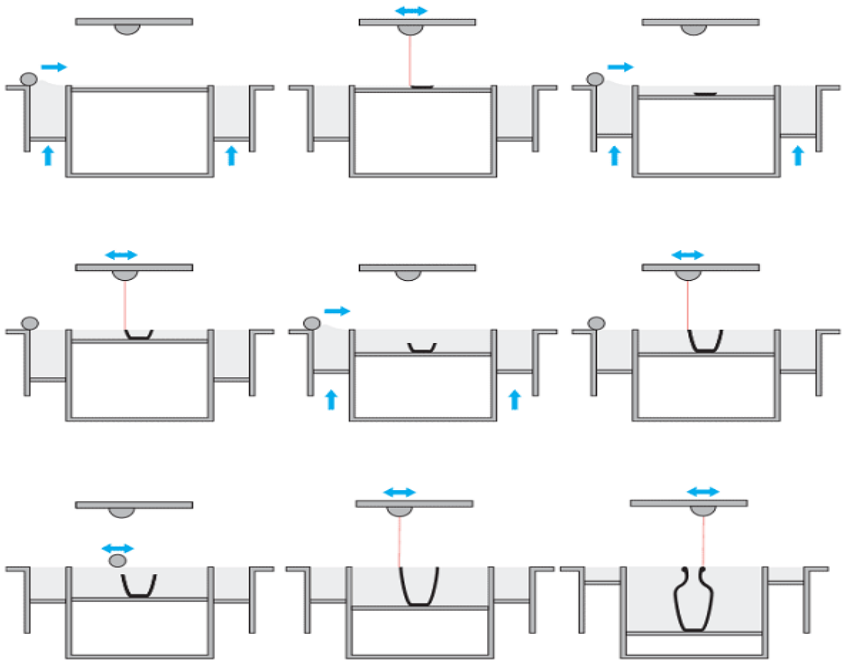

Figure 2 - Schematics of the direct laser metal sintering (i.materialise 2017)

2.2 Packed bed catalytic reactors

Packed bed reactors, as the name indicates, consist in a vessel with particles or a structured matrix inside, and have an important role in the chemical industry because they allow to achieve a high contact surface between the fluid and the solid phases while keeping low pressure drop along the catalyst bed (Edouard et al. 2009). Packed bed reactors have a variety of applications, such as adsorption, ion-exchange resin beds and heat exchangers (Allen, et al. 2013).

The properties of a packed bed reactor depend mostly on the packing matrix chosen to produce the reactor and how it was loaded. For a long time, the packing of the bed consisted in an art rather than science. The type of material chosen must have a high active surface area per unit volume, produce a low pressure drop, must be able to sustain abrasion and crushing, and yet be cheap. The voidage among particles in the reactor is also a very important parameter because the pressure drop is very sensitive

the mean porosity (ε), being roughly proportional to ε^{-3} (Afandizadeh and Foumeny 2001) as it can be seen in the typically used equation to predict the pressure drop for spherical particles, commonly known as Ergun's equation:

$$\Delta p = \frac{K_1 \, \mu \, L}{{d_p}^2} \frac{(1-\varepsilon)^2}{\varepsilon^3} v + \frac{K_2 \, L \, \rho}{d_p} \frac{1-\varepsilon}{\varepsilon^3} \, v^2 \, , \qquad (1)$$

where K_1 = 150 and K_2=1.75 are constants established via experimentation for spherical particles, μ is the fluid viscosity, v is the superficial velocity, L is the length of the bed, d_p is the diameter of the particles and ε is the porosity of the bed.

Packing beds are commonly filled with pellets in the shape of sphere or cylinders typically between 1.5 mm to 6 mm in diameter. Using smaller particles can cause a major pressure drop through the reactor, and larger sizes may lead to diffusion limitations (Bartal, et al. 2009).

In the case of the packed beds used as heat exchangers, the material chosen must also present a high thermal conductivity. The heat transfer coefficient can be influenced by the form of the particles, the velocity of the fluid and the operating temperature. Regarding the particles, the main parameter is the superficial area, because a high value will increase the conductive heat transfer rate (Suryanarayana, et al. 2011). The increase in velocity, and consequently in the flow rate, increases the convective heat transfer (Pešić, et al. 2014).

Packed beds used in catalytic converters and thermal energy storage present a low porosity, typically between 0.3 and 0.6. Due to the low porosity, a high pressure drop is obtained for high flows rates, which are required to maintain acceptable selectivity. In addition, the particles in the packed bed are not well connected to each other, only having local contact points, which reduces the effective thermal conductivity of the system (Edouard, et al. 2008).

An attractive alternative to overcome these drawbacks is the implementation of open-cell metal foams, because of their high surface area to volume ratio as well as enhanced flow mixing and attractive stiffness and strength (Mancin, et al. 2010). Also, the open porosity and low relative density makes the metal foam thermal management devices efficient, compact and lightweight.

These foams can be produced with different geometries and shapes, allowing to adjust the patterns of axial and radial flow. The small thickness of the cell struts allows the reduction of the diffusional limitations while enabling the decrease of secondary reactions and by-products (Edouard, et al. 2008). These foams can be described as

function of their cell size, strut thickness and porosity. These three aspects influence the specific surface area and in return the pressure drop, which are important characteristics for the reactor design. The specific area also influences momentum, heat, and mass transfer (Inayat, et al. 2011). Among the metals typically used, aluminium has emerged because of its low density, high thermal conductivity, and its relatively low price (Nawaz, et al. 2012).

The global heat transfer coefficient will depend mainly of the thermal conductivity and the heat convective coefficient. The first one is related with the heat transfer through the solid and the second to the heat transfer from or to the fluid. Radiation is only of importance for experiments realized at temperatures above 400 ºC.

The heat transfer in the foam-fluid will then depend on the porosity, thermal conductivity of the foam structure, fluid properties, geometrical parameters of the unit cells and operating temperature.

The increase in porosity leads to a decrease of the heat transfer rate, as this implies more free space in the packed bed and therefore a larger fraction of the heat has to be transferred by the fluid. Since metal conductivity is high, the global heat transfer coefficient will decrease with the increase of porosity. The same rationale can be applied to the strut thickness of the unit cell. The increase in the thickness will increase the amount of metal present in the foam, and decrease the porosity, therefore the global heat transfer will increase (Bianchi, et al. 2016).

Furthermore, the fluid used will also affect significantly the heat transfer rate because each fluid produces different convective heat coefficients, and liquids present a higher coefficient when compared to gases (Dyga and Płaczek 2015).

The operating temperature will also directly influence the global heat transfer, as a temperature increase will increase the driving force of heat transfer.

Packed beds in the form of foams are being used and studied for heterogeneous catalysis including the combustion of methane, the production of hydrogen gas via water-gas shift reaction, and the purification of exhaust gases from automotive engines (Giani, et al. 2005). A similar structure was developed in this work using 3D printing, more specifically using the direct laser metal sintering technique. The structures obtained consist of not only the foam, as in the examples before, but also contain the tube connected to the foam as shown in *Figure 3*.

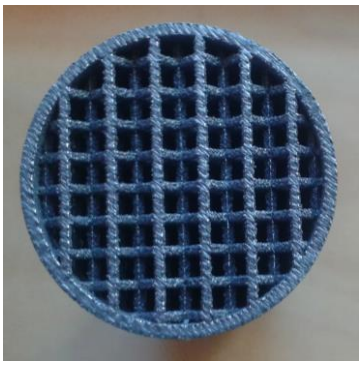

Figure 3 – Top view of the packed bed obtained through 3D printing

The packed structures used in this work consists of iso-reticular metallic cubic open cells, in which several parameters known to influence the pressure drop and heat transfer coefficient were varied. These parameters included the cell width, strut thickness and the angle of the cubes, and the focus of this work was the measurement of the pressure drop and the global heat transfer coefficient, since these are important aspects of the packed beds.

The knowledge of the pressure drop on these foam matrices is of vital importance for the design and operation of high performance industrial systems. In the past years, several experimental and theoretical works regarding the pressure drop of this type of structured foams have been published, mostly based in Ergun's type equation, yet all models so far fail to predict the pressure drop with high accuracy when no fitting of experimental data is available (Edouard, et al. 2008).

Even though the theoretical prediction may be difficult, it is known that the pressure drop increases significantly with the decrease of porosity. Therefore, it is expected that the pressure drop can be minimized in the cases where the porosity is higher and the cell size is larger or the strut width is smaller.

Another important aspect in this kind of reactors is the global heat transfer coefficient. Since, they can be used as a heat exchanger, it is important to have a high thermal conductivity and high heat capacity.

To carry out the calculations for the global heat transfer coefficient, the following assumptions were made: operation in steady state; constant material properties; incompressible fluid; negligible changes in the potential and kinetic energy

of the fluid; negligible axial heat transfer; homogeneous fluid temperature in the outer bath. Under these assumptions, the energy balance to the fluid becomes

$$\dot{Q} = \dot{m} C_{p,f} \Delta T \quad (2)$$

where $\dot{Q}$ is the heat transfer rate, $\dot{m}$ is the mass flow rate, $C_{p,f}$ is the fluid specific heat and ΔT is the change in the fluid temperature.

Furthermore, the heat rate exchanged between the packed bed and the fluid can be calculated as:

$$\dot{Q} = UA\Delta T_{LN} \quad (2)$$

where U is the global heat transfer coefficient, A is the contact area with the fluid and ΔT_{LN} is the log mean temperature difference which can be calculated as:

$$\Delta T_{LN} = \frac{T_{f,out} - T_{f,in}}{\ln\left(\frac{T_{wall} - T_{f,in}}{T_{wall} - T_{f,out}}\right)} \quad (3)$$

where $T_{f,in}$ and $T_{f,out}$ are respectively the temperature of the fluid in the entrance and exit of the packed bed, and the T_{wall} is the packed bed wall temperature assumed constant.

Combining *Eq. (2)* and *Eq (3)*, the following relation can be easily obtained:

$$U = \frac{\dot{m} C_{p,f} \Delta T}{\Delta T_{LN} A} \quad (4)$$

As stated before, with the increase in the velocity, a higher heat transfer coefficient will be achieved. Another important parameter is the contact area, since with its increase a higher heat transfer rate will also be achieved. Regarding the specifications of the cell, the following can be predicted: a smaller cell size will allow to obtain a higher surface area to contact with the fluid and consequently a higher heat transfer coefficient; for a higher cell strut width, the heat conduction will increase, which will be lean to an increase in the heat transfer coefficient.

3 Materials and Methods

In this thesis, the main focus was the study and characterization of different packed beds. These reactors consisted of open cell metal foams printed by direct laser metal sintering. The main material used was aluminium AlSi10Mg, but some were produced in stainless steel Ph1 for later comparison. All the cylindrical reactors were 10 cm in length (L), 2.54 cm of external diameter and 2.3 cm of internal diameter. The foam consisted of cubic cells, as exemplified in *Figure 4*.

As stated before, the main parameters in this kind of foams are the width of the cell and the strut thickness. The influence of the position of the cubes was also studied, by varying the angle relative to the reactor external tube, as can be seen in *Figure 5*.

For this study, seven foams were tested with the characteristics presented in *Table 1*.

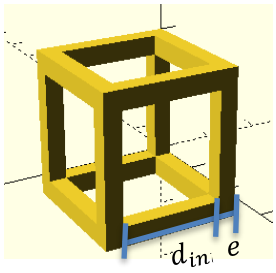

Figure 4 – Unit cell of the cubic foam

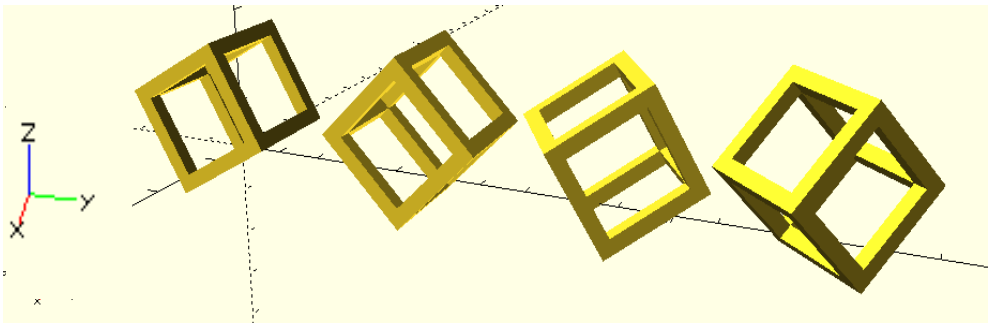

Figure 5 – Rotation of the unit cells in foams 3, 4, 5 and 6 (from left to right)

Table 1 – Characteristics of the foams

Foam number	Cell width (d_{int})	Strut thickness (e)	Rotation X axis	Rotation Z axis
1	1.5 mm	0.3 mm	45º	0º
2	2.0 mm	0.3 mm	45º	0º
3	2.0 mm	0.6 mm	30º	0º
4	2.0 mm	0.6 mm	45º	0º
5	2.0 mm	0.6 mm	30º	30º
6	2.0 mm	0.6 mm	45º	45º
7	2.0 mm	1.0 mm	45º	0º

Packings similar to reactors number 2, 4, 6 and 7 were also printed in stainless steel. The porosity was calculated assuming a periodic foam, and this means that the mean porosity of the bed should be the same as the porosity of one unit cell. So, the following equation was used:

$$\varepsilon = \frac{{d_{int}}^3 + 3\,{d_{int}}^2\,e}{(d_{int}+e)^3} \quad (5)$$

where, d_{int} is the cell width, e is the cell strut thickness and ε is the porosity.

To measure the real porosity of each foam, one end of the tube was taped with parafilm, the reactor filled with water and the weight difference measured. The porosity was calculated as:

$$\varepsilon = \frac{4\,\Delta m}{L\;{d_r}^2\,\pi\,\rho_f} \quad (6)$$

where Δm is the difference in its weight, ρ_f is the density of water, L is the bed length, and d_r is the internal diameter of the reactor.

3.1 Pressure drop and thermal capacity set up

In order to measure the pressure drop inside the 3D printed catalytic reactor, an installation was assembled, as illustrated in *Figure 6* and shown in *Figure 7*. To design the installation, it was necessary to have two points as close as possible to the extremities of the packed bed to measure the pressure drop, and an entrance to the

probe, and to be able to easily change the packed bed. Metal tubes were used in the inlet due to the high flow rates being used.

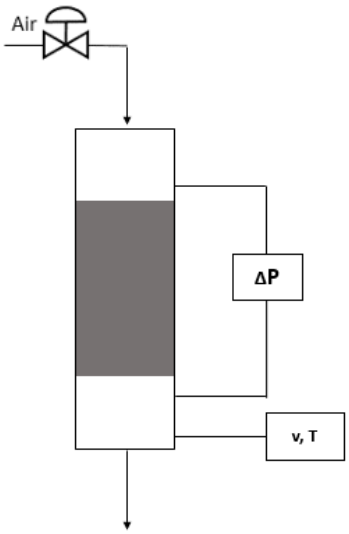

Figure 7 - Schematic of the experimental installation

Figure 6 – Experimental installation for the pressure drop measurement

During the experiments, the air flow was continuously increased and the following data was acquired: pressure drop (ΔP) measured using a differential pressure sensor (Testo 435-4), velocity (v) and temperature (T) measured using the attached velocity probe (Testo probe 0635 1025). The superficial velocity was varied between 0 and 20 $m \cdot s^{-1}$, measured at ambient pressure and temperature. The flow rate was initially measured to ensure the accuracy of the velocity values, and for this purpose a mass flow controller was used (El-Flow® Select for 50 L/min of air, Bronkhorst®).

Furthermore, the thermal capacity of the reactors was also measured and for that purpose the installation shown in *Figure 8* was used.

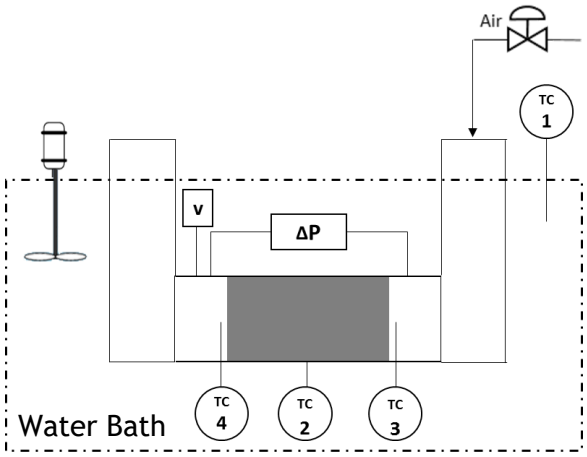

Figure 8 - Schematics of the installation used to measure the heat transfer coefficient

Similar to the previous one, it was necessary to measure the pressure drop as close as possible to the packed bed extremities, the velocity, and the temperatures in the water bath, the wall of the packed bed and at the entrance and exit of the packed bed. The main limitation in the design of the installation was the space in the water bath, so it was necessary to adapt to this size, requiring the use of a 90º curve.

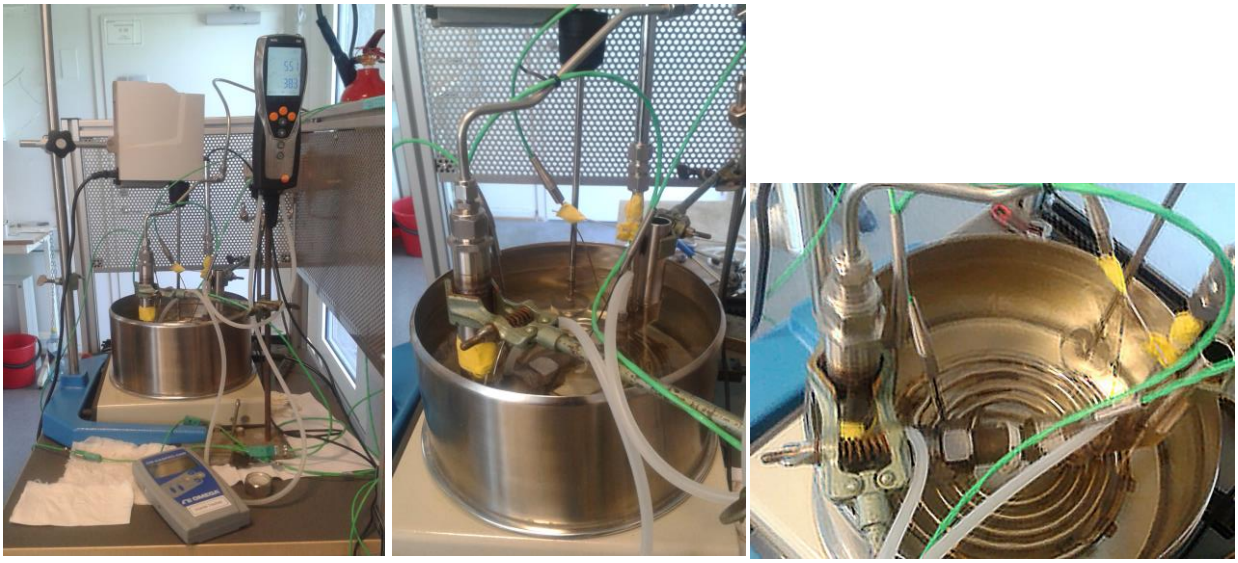

Figure 9 – Experimental installation for the thermal capacity

The installation was submerged in water and later heated at different temperatures, between 30 ºC and 70 ºC using a water bath (Büchi 471), using a digital overhead stirrer for medium-high viscosity liquids (DLH from VELP® scientifica) working at 760 rpm and later at 840 rpm to promote a good mixing of the water and therefore to homogenize efficiently the temperature in the water bath.

The temperatures were measured using thermocouples type K attached to a portable handheld Data Logger (DaqPro-5300 from Omega®). The thermocouples were located in the bath water ($TC1$), wall of the packed bed ($TC2$), and in the entrance ($TC3$) and exit ($TC4$) of the packed bed.

To accomplish a constant flow rate, the mass flow rate controller described before was used.

In addition, a design for a new structured packed bed was also created, but due to time limitations there was no opportunity to print it. This structured packed bed is shown in Appendix.

4 Results and discussion

The theoretical porosity was estimated using *Eq. (5)*, while the rendered porosity was obtained from the software Rhino with the file used to print the packed beds in order to determine the wall effect of adapting cubic cells to a cylindrical geometry. Both values were compared with the porosity obtained experimentally using *Eq. (6)* and the results are presented in *Table 2*.

Table 2 – Rendered and experimental porosity for each foam

Foam number	Theoretical Porosity	Rendered Porosity	Experimental Porosity
1	0.926	0.926	0.913
2	0.953	0.953	0.953
3	0.865	0.865	0.847
4	0.865	0.864	0.848
5	0.865	0.865	0.857
6	0.865	0.865	0.858
7	0.741	0.744	0.719

It can be observed that the theoretical values and the rendered values are very close, which confirms the periodic foam theory and the negligible effect of the local change of porosity in the reactor wall. Additionally, both values are close to the value obtained experimentally, with a maximum deviation of 3 %. It can be concluded that there were not a significant number of imperfect pores or broken ligaments during 3D printing, and that the accuracy of the printed parts is good.

Testing the response of the system to the air superficial velocity, the data shown in *Figure 11* were acquired in foam 4, and *Figure 10* shows the top view and the view at an angle of 45º.

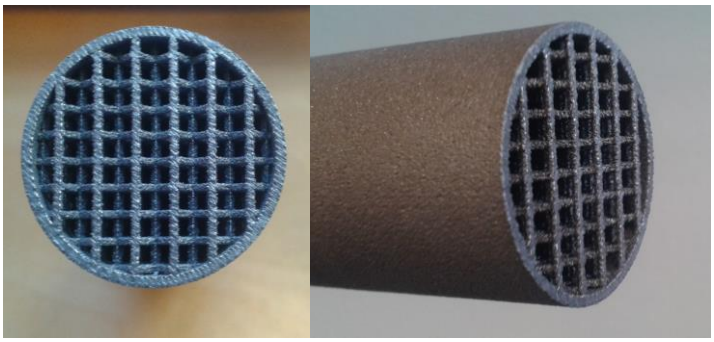

Figure 10 - Top view of foam 4 and respective view from a 45º angle

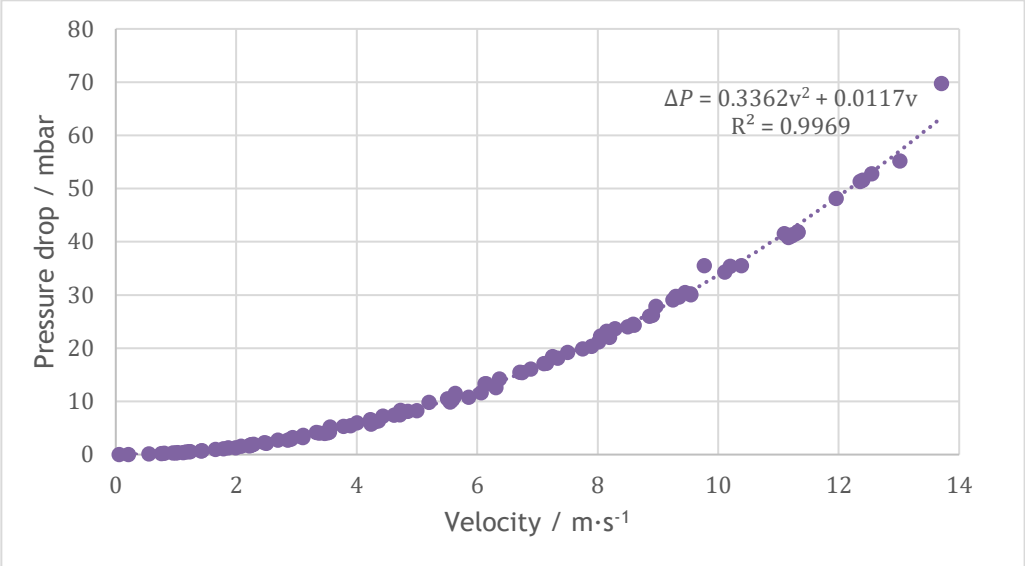

Figure 11 - Pressure drop as function of air superficial velocity in foam 4

From *Figure 11* it can be seen that the pressure drop increases as a polynomial function of second order. This represents the behaviour predicted by Ergun's equation (*Eq (1)*), in which the first term dominates in laminar flow and the second term in turbulent flow. With the increase of air velocity, the flow regime becomes more turbulent and the second term of the equation becomes dominant. This term varies with the square of the superficial velocity, so even if the velocity change is small, it will have a high impact in the pressure drop.

Using *Eq. (1)* it can be determined that the diameter of the spherical particles that would achieve the same pressure drop as foam 4 is d_p=1.6 mm.

After this initial test, the pressure drop for all packed beds was studied. All the packings consisted of hollow cubes of different sizes, angles, or material, those being the parameters studied.

The analysis begins with the influence of the cell size, and more specifically the unit cell width. For this purpose, two different packed beds were studied, one with cubes of 1.5 mm (Foam 1) and the other with cubes of 2 mm (Foam 2); the porosities are, respectively,

0.913 and 0.953. The results obtained are represented in *Figure 13*. The difference in these structures is visible in *Figure 12*.

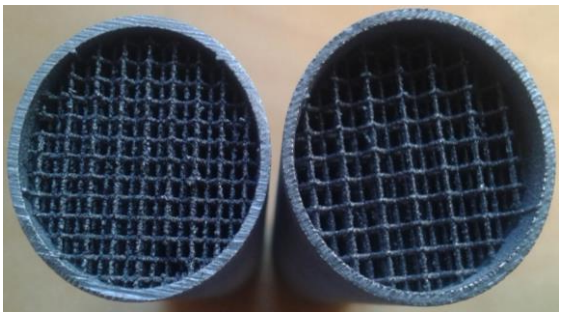

Figure 12 – Top view of foams 1 and 2 (left to right)

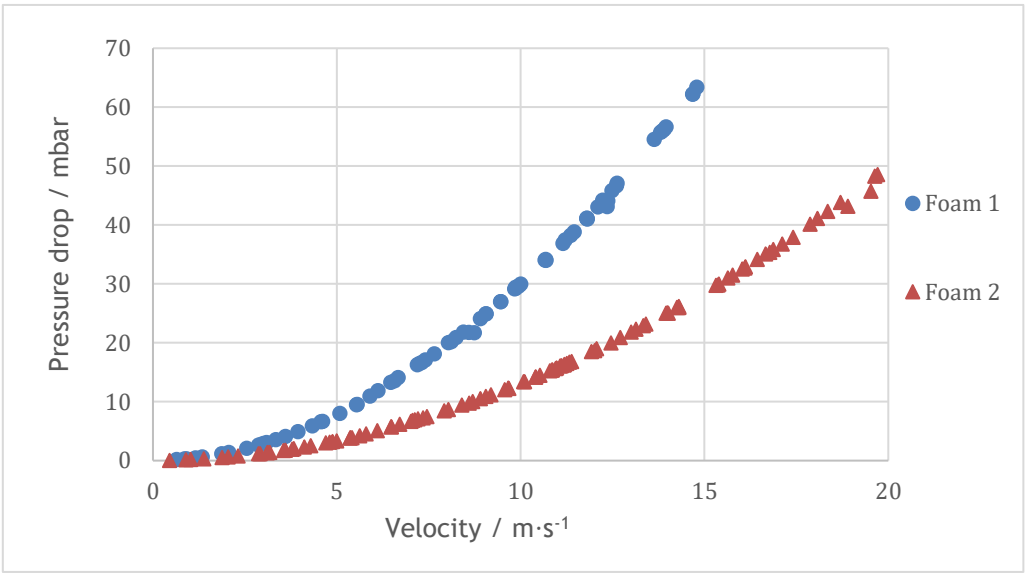

Figure 13 - Pressure drop as function of the air superficial velocity for cubes with different cell widths

Foam 1 presents a higher pressure drop, which can be explained based on two parameters intrinsically related, namely the lower porosity and the smaller cell size. As stated before, a smaller cell size and constant strut thickness implies a lower porosity, since there is a larger number of cells, per unit volume. Since the pressure drop is very sensitive to the porosity, this reactor presents a comparatively higher pressure drop.

In terms of size, the influence of the thickness of the cube struts was also studied. For that purpose, three packed beds were used, one with 0.3 mm (Foam 2), another with 0.6 mm (Foam 4) and finally one with 1 mm (Foam 7). Higher thicknesses implies a lower porosity, and consequently a higher pressure drop. This was confirmed by the results showed in *Figure 15*. *Figure 14* shows a top view of the foams, in which the different cube strut thicknesses are visible.

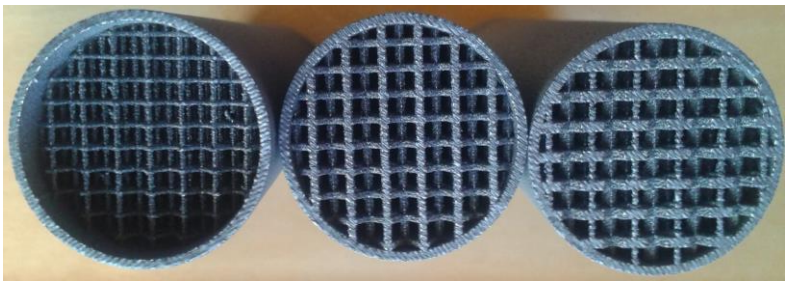

Figure 14 - Top view of the foams 2, 4 and 7 (from left to right)

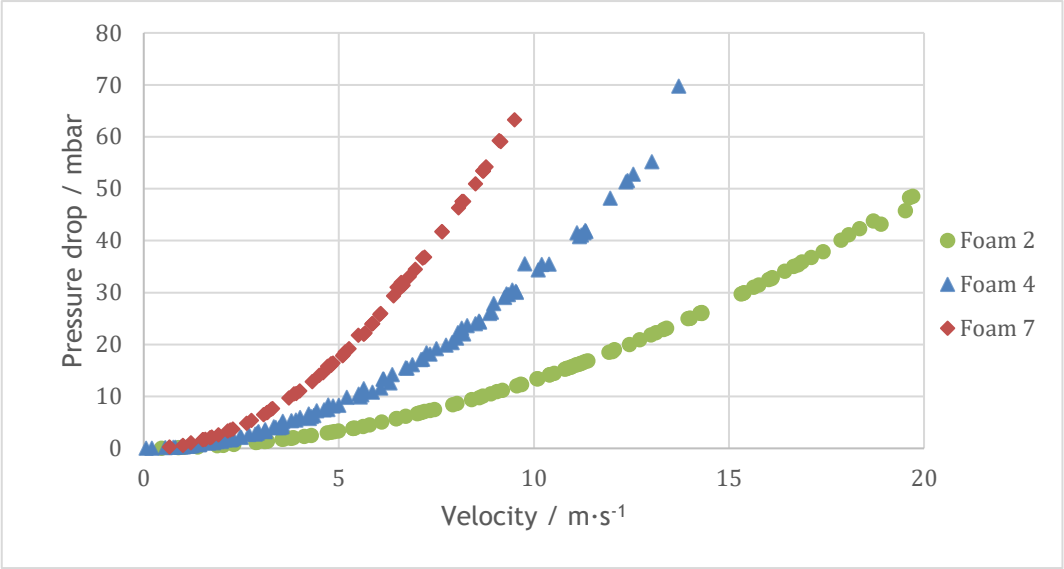

Figure 15 - Pressure drop as function of air superficial velocity for different thickness of the cube struts

The influence of the angle of the cubes was also studied. For this purpose, the used matrices were rotated: 30º in the X axis (Foam 3), 45º in the X axis (Foam 4), 30º in X axis and 30º in Z axis (Foam 5) and 45º in X axis and 45º in the Z axis (Foam 6). The results are presented in *Figure 17*, and *Figure 16* shows the top view of the foams used.

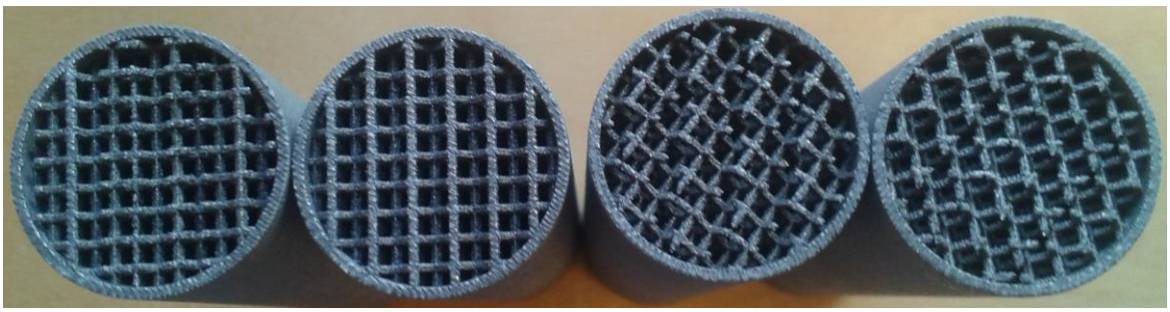

Figure 16 - Top view of foams 3, 4, 5 and 6 (from left to right)

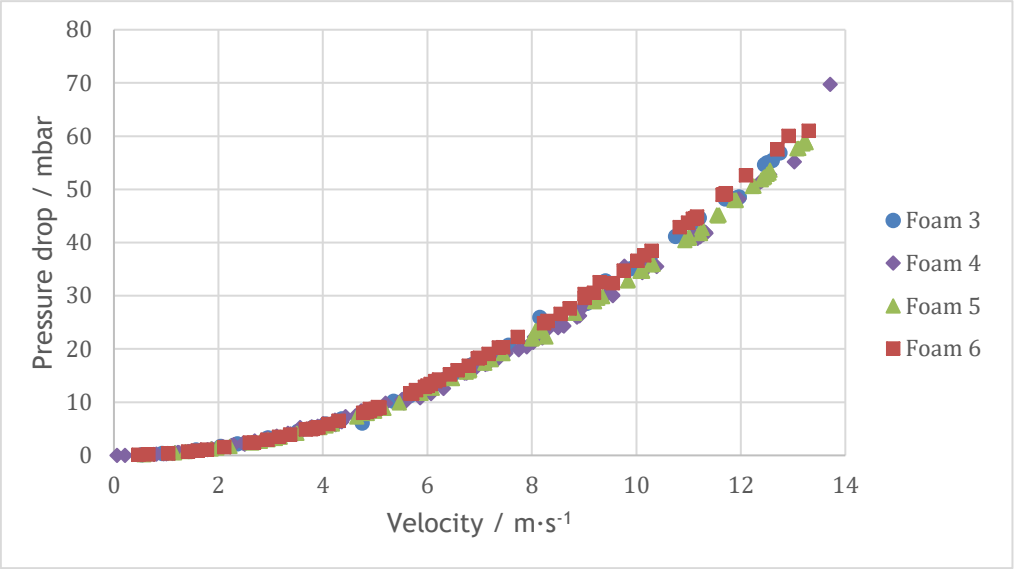

Figure 17 - Pressure drop as function of air superficial velocity in foams with different angles

From *Figure 17*, it is possible to conclude that the angle is not an important factor in the pressure drop, and the slightly differences at higher velocities could be explained due to the small difference in porosities measured experimentally and the accuracy of the measurements.

The results presented so far were all measured in aluminium packed beds. The influence of the material used in the packed beds was also assessed. When comparing the measured porosity between the aluminum and the stainless steel packed beds, data compiled in *Table 3*, it is clear that the stainless steel foams present higher porosity. This happens because the 3D printing of different materials has different levels of accuracy. In this case, the aluminum packed beds present a closer porosity to the one predicted from the rendering, so this 3D printing was more accurate. *Figure 18* presents the top view of all foams, although at naked eye no difference is visible.

Table 3 - Experimentally measured porosity for the aluminium and stainless steel packed beds

Foam number	Rendered Porosity	Aluminium porosity	Stainless steel porosity
2	0.953	0.953	0.997
4	0.864	0.848	0.904
6	0.865	0.858	0.901
7	0.744	0.719	0.778

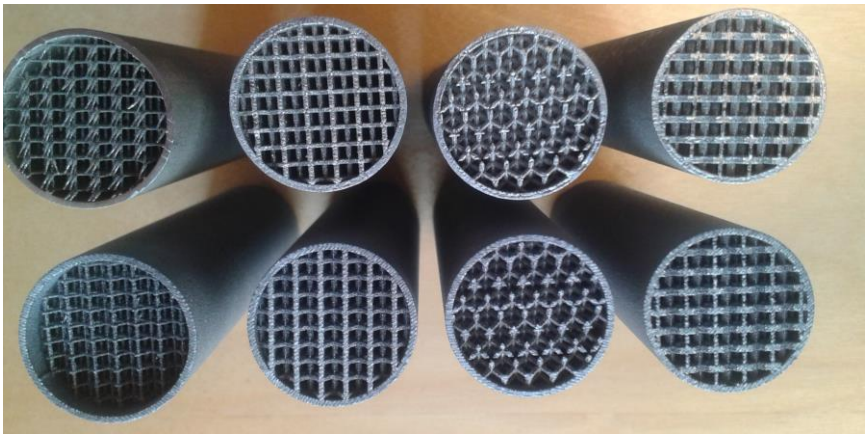

Figure 18 - Top view of foams 2, 4, 6 and 7 (from left to right). The stainless steel reactors are shown in the top row while in the bottom the aluminium reactors are shown.

Based on the measured porosity, it is expected that the pressure drop will be lower in the stainless steel reactors due to the higher porosity values. The results from these experiments are shown in *Figure 19*.

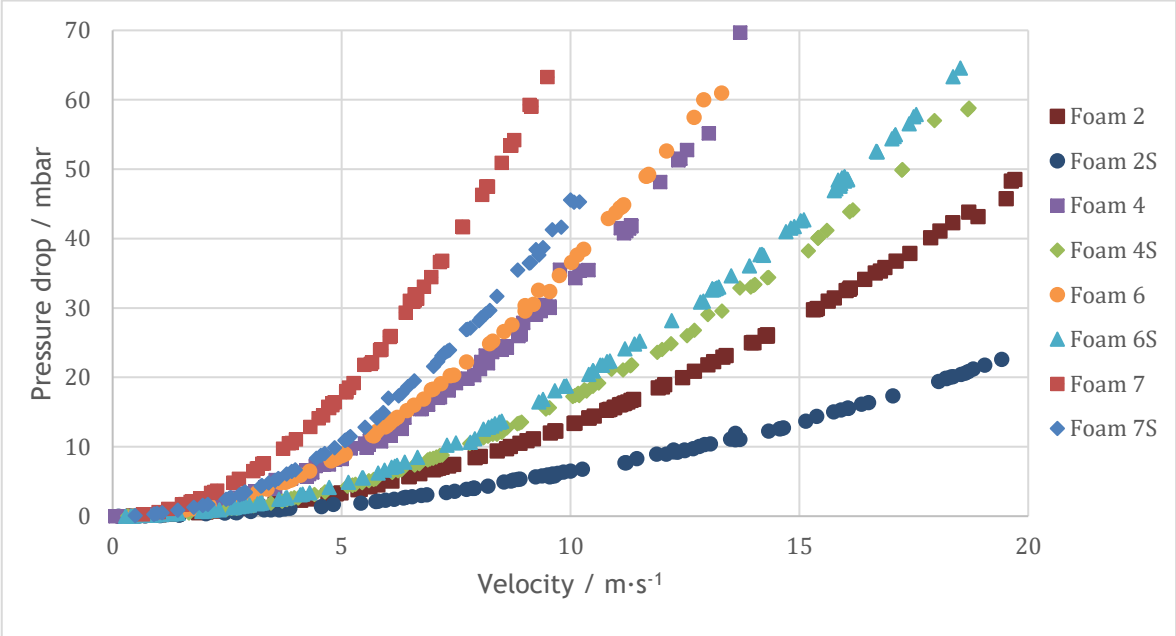

Figure 19 - Pressure drop as function of air superficial velocity comparing the different materials. The stainless steel foams are indicated by the S after the number

As expected, the pressure drop is lower in the stainless steel reactors, and besides this fact, the behaviour among both materials is similar. For a constant air velocity, the pressure drop increases as the porosity decreases, independently of the material used (as it can be seen in the appendix in *Figure 25* and *Figure 26*).

Next, we present the results obtained for the global heat transfer coefficient. The parameters investigated were: temperature of the outer bath, air superficial velocity, angle of the cubes, cell width and cell strut thickness.

Starting with the temperature of the bath it is expected that a higher temperature of the water bath will increase the heat transfer rate, since it will affect the foam temperature and the thermodynamic properties of both solid and fluid. The results obtained for the global heat transfer coefficient are presented in *Table 4*, calculated using *Eq (4)*. Since the superficial area of each foam is not easily measured, the results are presented as the global heat transfer coefficient times the area (UA). In this study, the same packed bed was always used, so the fact that the superficial area is unknown will not affect the comparison between the results, since the area is the same in all trials and therefore the global heat transfer coefficient can be directly compared. The results presented in *Table 4* correspond to a stirring speed of 720 rpm, while the remaining results presented are for 840 rpm.

Table 4 – Global heat transfer as function of the temperature of the water bath

Temperature (ºC)	Air superficial velocity ($m \cdot s^{-1}$)	UA ($W \cdot K^{-1}$)
39.1	4.09	2.63
52.9	4.32	2.86
64.8	4.30	3.16
69.6	4.46	3.01

As expected, using higher bath temperatures leads to a higher temperature in the foam and therefore the increase in the heat transfer rate of the material. With the increase in the solid conductivity, it is possible to achieve a higher global heat transfer rate. The two points at higher bath temperature shown in Table 4 do not fit with the trend, but this can be explained due to the small difference between the fluid exit temperature and the bath temperature. Since both are so close, a small difference in the temperature measurement can have a great impact in the final result.

The influence of the air velocity was studied and, as expected, the increase in the air flow rate leads to a more turbulent flow which increases the convective heat transfer coefficient, as shown in *Figure 20*.

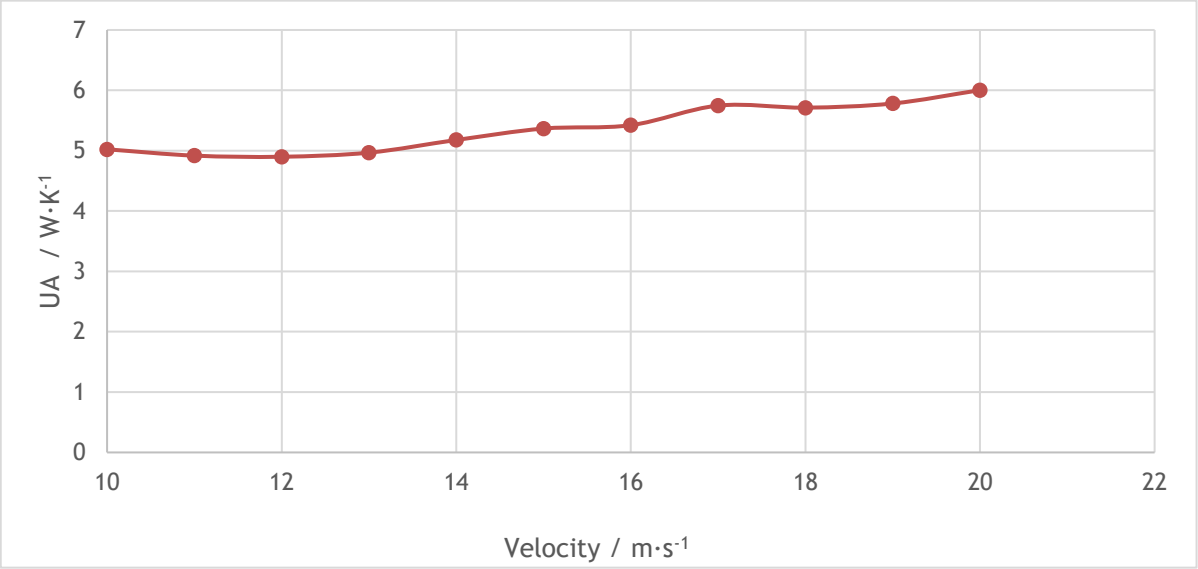

Figure 20 - UA as function of air superficial velocity in foam 4. The water bath temperature was 71.0 ºC

The cell size of the foam was also studied, to assess the influence on the global heat transfer coefficient, and the results are presented in *Figure 21*. The foams used were foam 1, with 1.5 mm, and foam 2 with 2.0 mm.

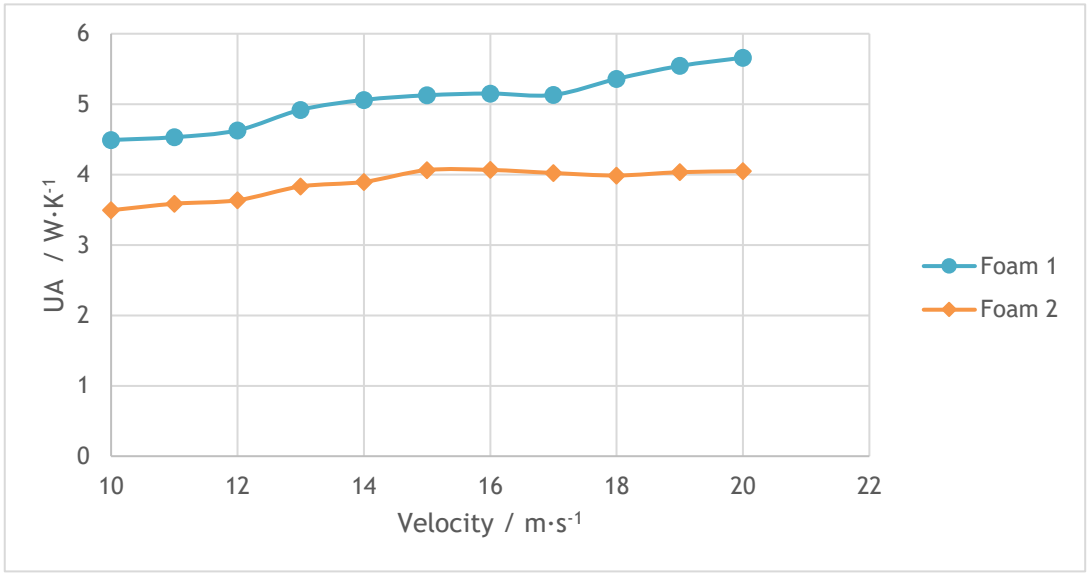

Figure 21 - UA as function of air superficial velocity for foams 1 and 2 with different cell width, and the water bath temperature was 74.2 ºC and 74.9 ºC respectively

Figure 21 shows that cells with a smaller width present higher global heat transfer coefficients. The smaller width will decrease the porosity and thus increase the contact points between foam and fluid. This way, the global heat transfer increases, since the conductive process in the foam is very important to the global heat transfer.

In addition, in foam 2 the UA values for velocities above 16 m·s^{-1} are nearly constant, around a value of 4.04 W·K^{-1}. Therefore, it can be proposed that for higher velocities the metal packed structure has reached its maximum heat transfer capability, and thus the heat transfer from the water bath to the fluid will remain the same independently of the fluid velocity. So, the heat transfer is now limited due to the conductive heat transfer of the packed bed.

The influence of the thickness of the strut was also studied. It can be predicted that the thicker the cell strut, the higher the global heat transfer coefficients. The experimental results are shown in *Figure 22*.

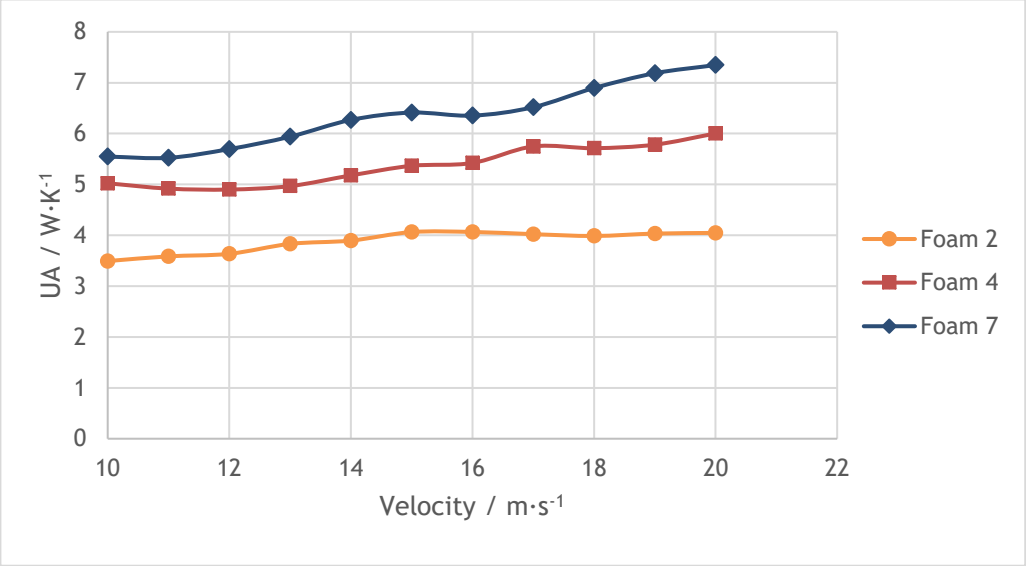

Figure 22 - UA as function of the air superficial velocity for foams with different strut thicknesses

As expected, the global heat transfer increased with the increase of the strut thickness. This can be easily explained since the metal conductive capability is higher increasing the strut thickness. Therefore, a thicker strut will create a foam with smaller porosity and a greater part of the heat can be transferred by conduction through the metal, allowing to achieve a higher global heat transfer coefficient.

Finally, the influence of the angle of the cubic matrix was studied, and the results are presented in *Figure 23*.

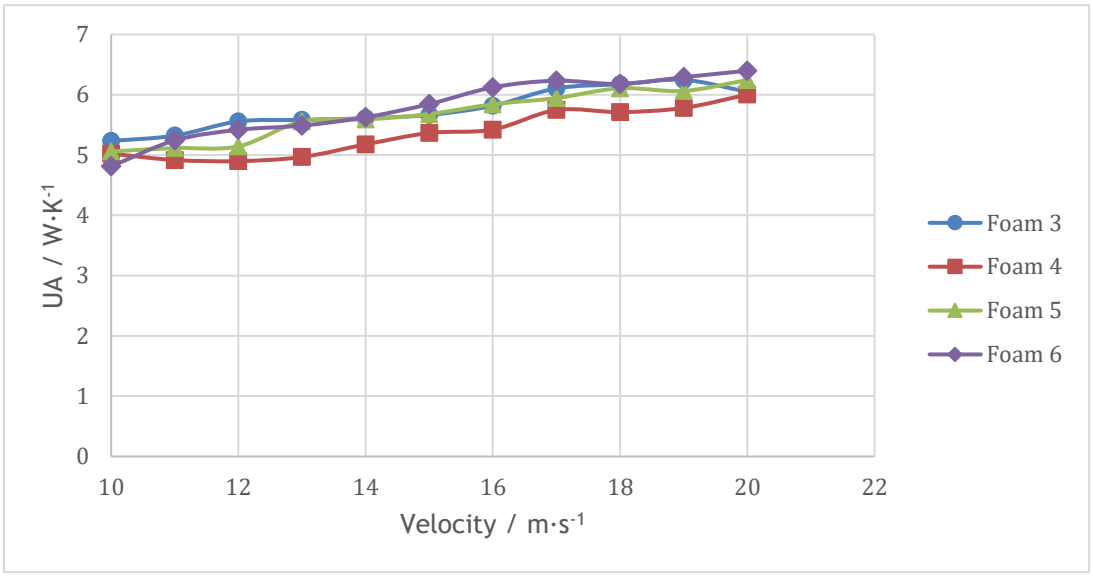

Figure 23 - UA as function of air superficial velocity for different angles of the cubic matrix

As it can be seen, the results were similar in all foams and this again shows that the angle is not a major parameter in the design of the packed beds. Furthermore, the small difference between the data sets shown in *Figure 23* can be explained due to the slight difference in the porosity, the slightly different temperatures of the water bath, and the errors associated to the measurements.

Comparing between all parameters analysed before, all the experimental data was represented in *Figure 24*.

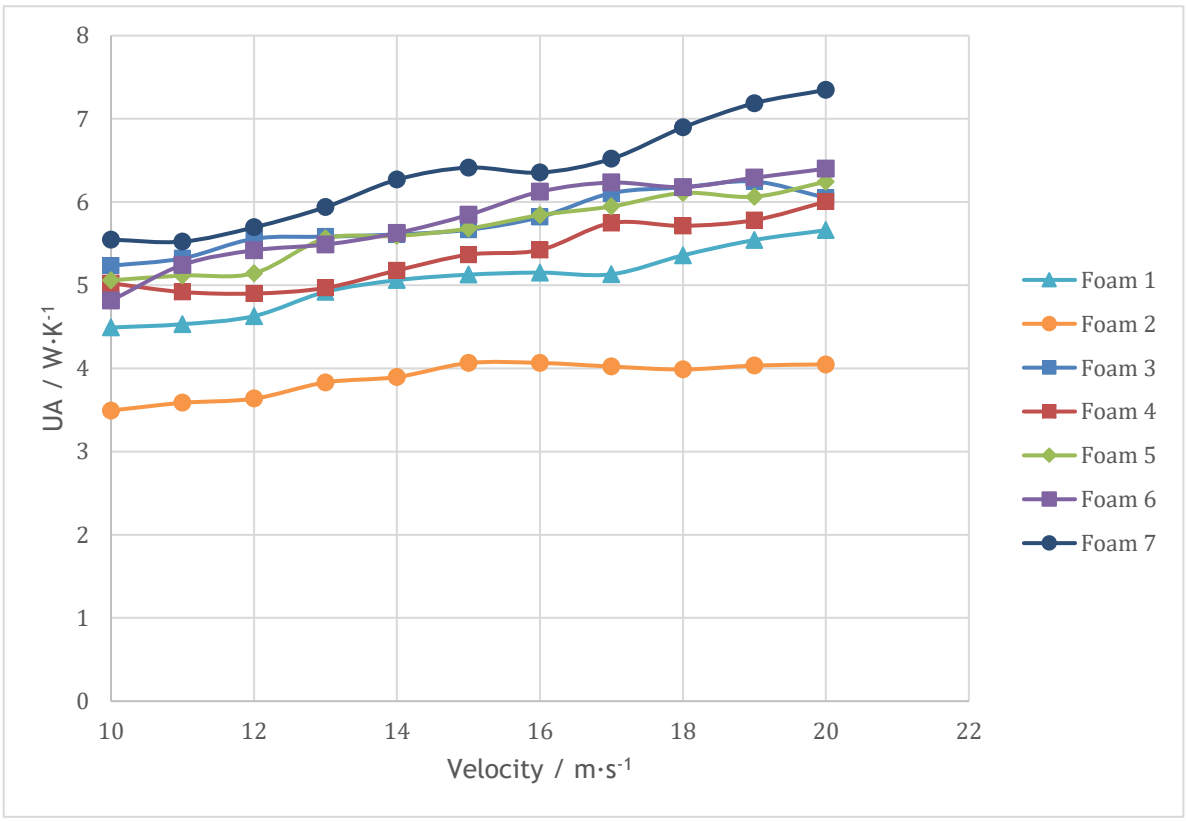

Figure 24 - UA as function of the air superficial velocity in all foams

From the analysis, it can be concluded that the main parameter influencing the global heat transfer coefficient is the strut thickness, since the higher and lower *UA* values correspond to the extremes of this parameter. Furthermore, it can also be seen that foam 1 has a coefficient close to the foam 4, so it can be assumed that even though it presents a lower strut thickness, the increase in the contact area allows to overcome this effect and leads to similar results compared to the other structured beds.

5 Conclusions

Classical packed bed reactors consist in vessels with particles in the interior, and over the years several studies have been developed to improve them. The main focus of such studies are typically about the pressure drop and the heat exchange. Classical packed beds consisted of particles but more recent studies demonstrated that metal open cells foams allow to achieve better results in both fields.

In terms of pressure drop, the results obtained in this work were consistent with the expected ones. The lowest pressure drop was obtained with higher porosity, higher cell sizes, and smaller strut thickness. Furthermore, the accuracy of the 3D printing using different materials was illustrated as the same design of reactor resulted in structures with different porosities.

The second objective was the study of the heat transfer coefficient. Again, the behavior observed agrees with the expected results. The experimental results show that the global heat transfer coefficient is higher for higher velocities, smaller cell size and larger strut thickness. The last two parameters directly influence the specific contact area between the solid and the liquid, which is one of the most important aspects in the heat transfer along with the material used in the foam structure.

In summary, the objectives of this dissertation were achieved, since it was shown using the foams available which are the best designs to achieve lower pressure drop and higher global heat transfer coefficient. The foam with lower pressure drop was foam 2, while the foam with the better performance in terms of global heat transfer coefficient was foam 7.

6 Assessment of the work done

6.1 Objectives achieved

The main objectives for this work were the experimental characterization of several foams in terms of pressure drop and global heat transfer coefficient. Both topics were analyzed in detail and the conclusions obtained for each of the parameters studied were presented and were coherent to the expected behavior.

6.2 Limitations and suggestions for future work

The main limitations in this work were the difficulty to achieve the same operating conditions in each experiment, as the temperature and the velocity change with time. The experimental determination of the superficial area would allow to directly compare the heat transfer between different foams.

Suggestions for future work are the comparison of the experimental data with modeling using CFD, and the test of different structured foams, such as foams created with Kelvin cells or Weaire–Phelan structures.

These type of foams can be introduced in tubular heat exchangers or can be used as structures for fixed bed reactors, and in both cases can lead to important advantages.

References

Afandizadeh, S., and E.A Foumeny. “Design of packed bed reactors: guides to catalyst shape, size, and loading selection.” *Applied Thermal Engineering 21*, 2001: 669-682.

Allen, K.G., T.W. von Backström, and D.G. Kröger. “Packed bed pressure drop dependence on particle shape, size distribution, packing arrangement and roughness.” *Powder Technology 246*, 2013: 590-600.

Bartal, Nicholas, Gabriella Serrati, Daniel Szewczyk, and John Waterman. “Modeling of a Catalytic Packed Bed Reactor and Gas Chromatograph Using COMSOL Multiphysics.” 2009.

Bianchi, Enrico, Wilhelm Schwieger, and Hannsjorg Freund. "Assessment of Periodic Open Cellular Structures for Enhanced Heat Conduction in Catalytic Fixed-Bed Reactors." *Advanced Engineering Materials*, 2016: 608-614.

Cotteleer, Mark, and Jim Joyce. *3D opportunity: Additive manufacturing paths to performance, innovation, and growth*. 17 January 2014. https://dupress.deloitte.com/dup-us-en/deloitte-review/issue-14/dr14-3d-opportunity.html.

Dodziuk, Helena. *What’s New in 3D Printing?* 12 Fevereiro 2014. http://www.chemistryviews.org/details/ezine/5736441/Whats_New_in_3D_Printing.html.

Dukhan, N. “Correlations for the pressure drop for flow through metal foam.” *Experiments in Fluids 41*, 2006: 665-672.

Dyga, Roman, and Małgorzata Płaczek. "Heat transfer through metal foam–fluid system." *Experimental Thermal and Fluid Science, Volume 65*, 2015: 1-12.

Edouard, David, Maxime Lacroix, Cuong Pham Huu, and Francis Luck. “Pressure drop modeling on SOLID foam: State-of-the art correlation.” *Chemical Engineering Journal, Volume 144*, 2008: 299-311.

Edouard, David, Svetlana Ivanova, Maxime Lacroix, Estelle Vanhaecke, Charlotte Pham, and Cuong Pham-Huu. “Pressure drop measurements and hydrodynamic model description of SiC foam com posites decorated with SiC nanofiber.” *Catalysis Today 141*, 2009: 403-408.

Ford, Simon, and Mélanie Despeisse. “Additive manufacturing and sustainability: an exploratory study of the advantages and challenges.” *Journal of Cleaner Production 137*, 2016: 1573-1587.

GE Additive. *GE Additive*. 15 November 2016. http://www.geadditive.com/press-releases/ge-additive-manufacturing-in-alabama-future-is-now (accessed June 8, 2017).

Giani, Leonardo, Gianpiero Groppi, and Enrico Tronconi. "Mass-Transfer Characterization of Metallic Foams as Supports for Structured Catalysts." *Ind. Eng. Chem. Res. 44*, 2005: 4993-5002.

i.materialise. 19 April 2017. https://i.materialise.com/blog/direct-metal-laser-sintering-dmls/ (accessed Maio 26, 2017).

Inayat, Amer, Hannsjorg Freund, Andreas Schwab, Thomas Zeiser, and Wilhelm Schwieger. "Predicting the Specific Surface Area and Pressure Drop of Reticulated Ceramic Foams Used as Catalyst Support." *Advanced Engineering Materials 11*, 2011: 990-995.

Mancin, Simone, Claudio Zilio, Alberto Cavallini, and Luisa Rossetto. "Pressure drop during air flow in aluminum foams." *International Journal of Heat and Mass Transfer 53*, 2010: 3121-3130.

Metal AM. n.d. http://www.metal-am.com/introduction-to-metal-additive-manufacturing-and-3d-printing/applications-for-additive-manufacturing-technology/ (accessed June 8, 2017).

Nadgorny, Milena, Zeyun Xiao, Chao Chen, and Luke A. Connal. "Three-Dimensional Printing of pH-Responsive and Functional Polymers on an Affordable Desktop Printer." *Applied Materials & Interfaces, Volume 8*, 2016: 28946 - 28954.

Nawaz, Kashif, Jessica Bock, and Anthony M. Jacobi. "Thermal-Hydraulic Performance of Metal Foam Heat Exchangers." *International Refrigeration and Air Conditioning Conference*, 2012.

Pešić, Radojica, Tatjana K Radoicˇić, Nevenka Bošković -Vragolovic, Zorana Arsenijević, and Zˇeljko Grbavcˇić. "Heat transfer between a packed bed and a larger immersed spherical particle." *International Journal of Heat and Mass Transfer*, 2014: 130-136.

Rockstroh, Todd, Dave Abbott, Ken Hix, and Josh Mook. "Lessons learned from development cycle." *Industrial Laser Solutions, Volume 28*, 2013.

Sivertsen, Espen. *Type A Machines - Manufacturing the future*. 30 September 2016. https://www.typeamachines.com/blog/a-brief-history-of-additive-manufacturing (accessed June 8, 2017).

Suryanarayana, K. V., G. Srinivasa Rao, D. M. Reddy Pasad, K. V. Sharma, and P. K. Sarma. "Experimental analysis of heat and mass transfer in a packed bed." *Journal of Mechanical Engineering and Sciences, Volume 1*, 2011: 124-132.

Tommaso, Cavallini. “Experimental and numerical study of heat transfer in open cell metal foam as catalyst support.” Thesis, 2014.

Van Thienen, Stefan, Andrew Clinton, Monika Mahto, and Brenna Sniderman. *Industry 4.0 and the chemicals industry - Catalyzing transformation through operations improvement and business growth*. Deloitte University Press, 2016.

Appendix 1

Properties of the packed beds

Table 5 – Properties of all aluminium foams

		Foam 1	Foam 2	Foam 3	Foam 4	Foam 5	Foam 6	Foam 7
d_r		2.3 cm						
L		10.1 cm						
d_{int} (mm)		1.5	2.0	2.0	2.0	2.0	2.0	2.0
e (mm)		0.3	0.3	0.6	0.6	0.6	0.6	1.0
Angle	X axis	45°	45°	30°	45°	30°	45°	45°
	Z axis	0°	0°	0°	0°	30°	45°	0°
Δm (g)		38.225	39.905	35.485	35.345	35.905	35.945	30.105
ε_e		0.913	0.953	0.847	0.848	0.857	0.858	0.719

Table 6 – Properties of all the stainless steel foams

		Foam 2S	Foam 4S	Foam 6S	Foam 7S
d_r		2.3 cm			
L		10.1 cm			
d_{int} (mm)		2.0	2.0	2.0	2.0
e (mm)		0.3	0.6	0.6	1.0
Angle	X axis	45°	45°	45°	45°
	Z axis	0°	0°	45°	0°
Δm (g)		42.995	37.745	37.875	32.600
ε_e		0.997	0.901	0.904	0.778

Pressure drop in the stainless steel foams

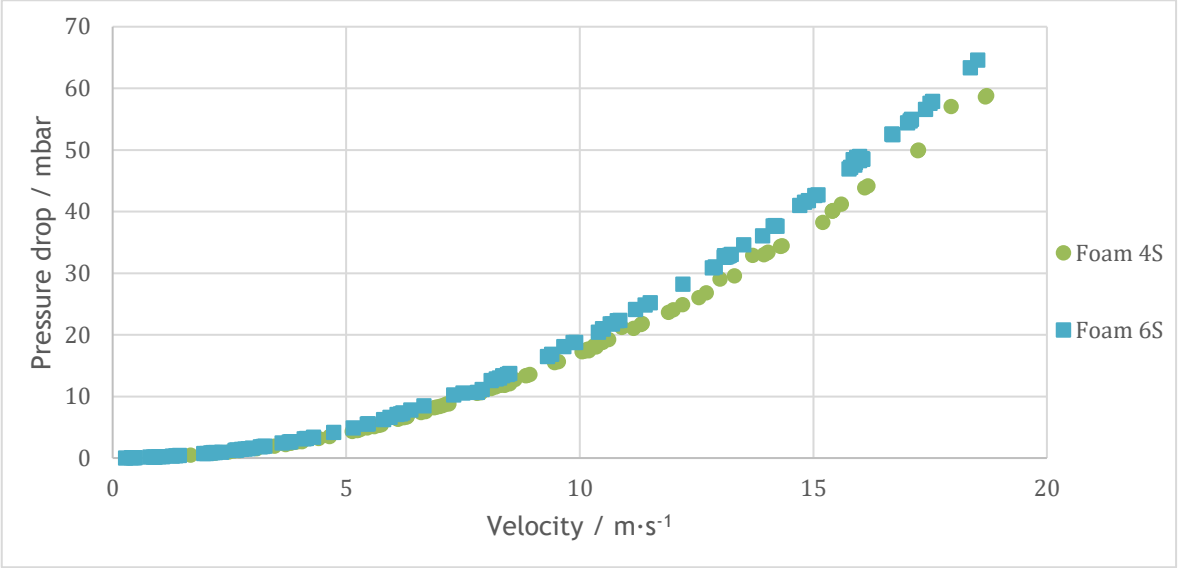

Figure 25 - Pressure drop as function of air superficial velocity in foams with different angles in stainless steel foam

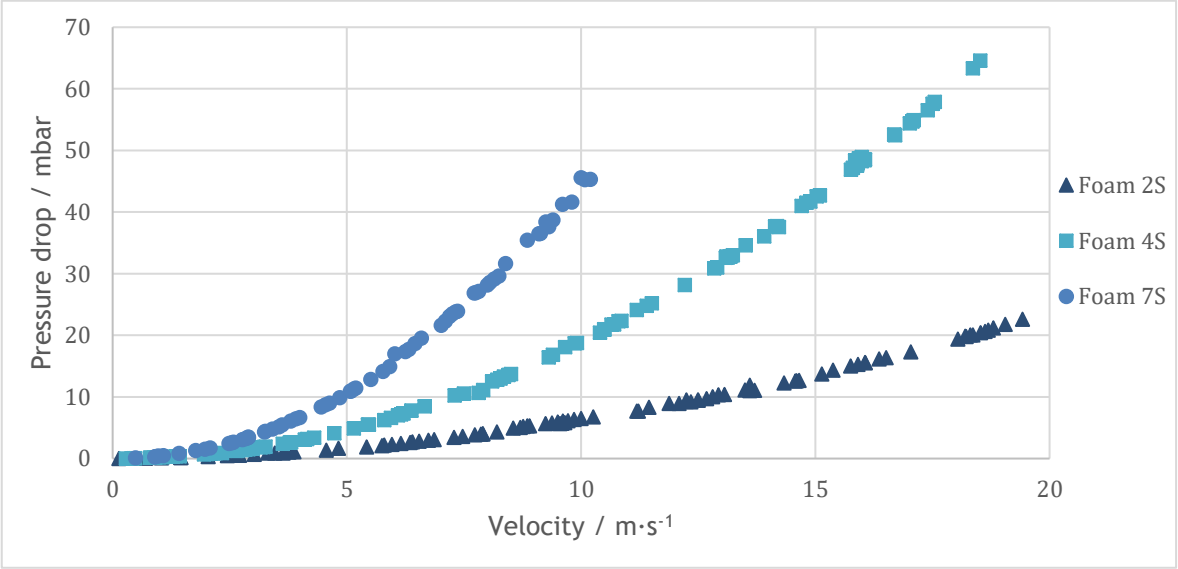

Figure 26 - Pressure drop as function of air superficial velocity for different thicknesses of the cube struts in the stainless steel foam

Proposed packed bed structure

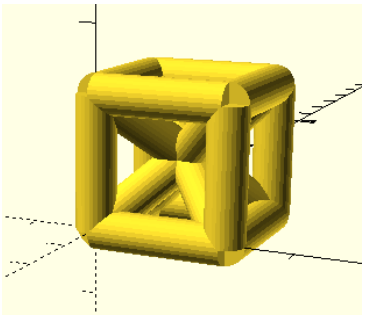

Figure 27 – Unit cell of the proposed packed bed

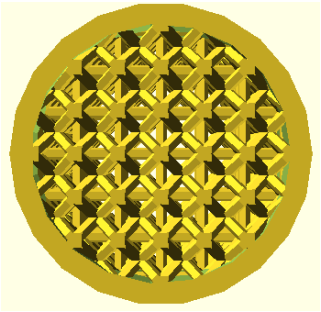

Figure 28 - Top view of the proposed packed bed